J. Fluid Mech. (1971), *vol.* 45, *part* 1, *pp.* 91–110
Printed in Great Britain

Linear stability of the dissipative, two-fluid, cylindrical Couette problem. Part 1. The stably-stratified hydrodynamic problem

By G. P. SCHNEYER† AND S. A. BERGER
Aeronautical Sciences Division, University of California, Berkeley

(Received 17 July 1969 and in revised form 20 July 1970)

The stability of a two-fluid vortex is studied as a step towards understanding the separation and containment problems in a gaseous-core nuclear rocket. In particular, the linear hydrodynamic stability of two incompressible, immiscible, viscous fluids occupying separate annular regions of a cylindrical Couette apparatus is considered. Neglecting surface tension and gravity, a conservative assumption, the governing equations for arbitrary jumps in fluid properties are derived and numerical solutions to the resultant eigenvalue problems obtained. Results are presented for the effect on neutral stability of density and viscosity jumps, varying gap widths, and differing fluid–fluid interfacial positions. The solutions are limited, however, to the case of stably stratified fluids and a stationary outer cylinder.

Two separate modes (multiple eigenvalues) have been discovered for all cases in which two fluids, differing in any property, are present. A rationale is presented for this phenomenon as well as for most of the other observed results.

While most results are believed to be manifestations of the Taylor cylindrical Couette instability phenomenon, evidence is presented for the existence of additional 'hidden' eigenvalues attributable to the classical Kelvin–Helmholtz and/or the recently reported Yih viscosity-stratification instability phenomena.

1. Introduction

(*a*) *Motivation*

Over the past decade several hydrodynamic vortex schemes have been proposed to help solve the separation and containment problems of gas-core nuclear rockets. This paper is the first step in analyzing the hydrodynamic stability of the MHD vortex system proposed by Johnson (1966). In this concept a reactor cavity is formed by concentric cylindrical electrodes, with annular regions of propellant (hydrogen), fuel (uranium), and propellant, respectively, filling the cavity. An axial magnetic field is applied, and a radial current drawn. As a result the fluid is accelerated azimuthally so that a three-region, two-fluid vortex is formed.

All containment schemes aim at increasing the fuel residence time while maintaining the desired propellant flow rate. This can be accomplished, theoretically at least, by maintaining separation of the fuel and propellant during the

† Present address: Mathematics Department, Imperial College, London.

flow process. In the Johnson (1966) system, the separation is achieved by balancing centrifugal and radial pressure forces in the vortex. In the analysis presented here it has been assumed that the flow rate requirements yield axial velocities small compared to the calculated azimuthal velocities, and axial Reynolds numbers small compared to the critical values for annular pipe flow. The latter requirement makes the axial velocity a stabilizing influence on the cylindrical Couette instability (Di Prima 1960; Hughes & Reid 1968), while the former tends to ensure that any Kelvin–Helmholtz instability due to the axial velocity distribution will be damped out by the strong radial pressure gradient (Chandrasekhar 1961). Thus, neglect of any axial body force or pressure gradient should be conservative.

The expected instability phenomena are related to centrifugal forces, shear, and the large density and viscosity gradients. Questions to be answered involve the relative importance of these phenomena, the adequacy of the axial magnetic field as a stabilizing factor, especially in a dissipative environment, and the trend effects of various parameters on stability. All of these questions can be studied by considering the model problem of a classical cylindrical Couette apparatus with two annular fluid regions and an applied axial magnetic field. This model does, admittedly, substitute mechanical rotation for the Lorentz force-induced rotation and does ignore the effects of radial current, axial flow and finite length (i.e. Ekman layer interactions), but it also provides a manageable, albeit complicated, approximation to a difficult problem. Furthermore, this model should yield some answers to all of the aforementioned questions.

The stably stratified (heavy outer fluid) case can be investigated via neutral stability curves whereas the unstably stratified version requires the calculation of growth rates, at least when MHD effects are negligible. As a consequence of this difference, as well as the scope of the full problem, the investigation has been divided into three parts. This paper reports on the stably stratified case without MHD effects. A computer program is already available to evaluate the changes due to MHD effects, while work on the unstably stratified problem is to be taken up in the future.

(*b*) *Earlier work*

The cylindrical Couette problem was first considered by Lord Rayleigh (1920), who investigated the inviscid, one-fluid problem from a heuristic viewpoint. He concluded that the flow is stable if and only if the square of the circulation (Γ^2) always rises with increasing radius. Taylor (1923) examined the viscous, narrow-gap version of this problem theoretically and experimentally and found that when a physically significant parameter (now termed the Taylor number and related to the ratio of rotational to viscous forces) exceeded a critical value, instability resulted. Following Taylor, many papers were written describing experiments and/or linear stability analyses using several different techniques on variations of Taylor's problem. This body of work culminated in the monumental treatise of Chandrasekhar (1961), whose bibliography quite adequately covers the literature to that date.

Subsequent theoretical work can be divided into narrow and wide gap analyses. Some of the narrow gap analyses include investigation of radial density variations

(Yih 1961; Pao 1966) and superposed axial flow (Di Prima 1960; Hughes & Reid 1968) among other effects. Some of the wide gap analyses have considered Taylor's original problem, with or without assuming axisymmetric perturbations, for various ranges of parameters (Krueger, Gross & Di Prima 1966; Gross 1965; Roberts 1965; and Sparrow, Munro & Jonsson 1964). A wide gap analysis of a case with radial density variations due to a temperature gradient has also been published (Walowit, Tsao & Di Prima 1964).

The experimental area has developed very rapidly since 1961. Among the prominent contributors (with representative papers) are Donnelly (Donnelly & Schwarz 1965), Snyder (Snyder & Lambert 1966), and Coles (1965). Although generally limited to narrow gap widths and a single fluid, these investigators have reported on a large variety of linear and non-linear, laminar and turbulent phenomena.

Recently, a non-linear analysis of Taylor's problem (Davey, Di Prima & Stuart 1968) has shown how the Taylor vortices become unstable at larger (supercritical) Taylor numbers, and thus has partially explained the experimental observations of Taylor (1923) and Coles (1965).

In the area of two-fluid problems, the classical analyses of the Rayleigh–Taylor (R–T) and Kelvin–Helmholtz (K–H) instabilities (involving rectilinear flows) are well covered by Chandrasekhar (1961), and Yih (1967) has recently reported an instability, henceforth called the Yih instability, which is generated by a stratification in viscosity. Finally, an inviscid analysis of a two-fluid, wide-gap cylindrical Couette apparatus has been reported (Reshotko & Monnin 1965) but, aside from the limitation to non-dissipative flow, the authors failed to allow for motion of the fluid–fluid interface, so that their conclusions may be in error.

In this paper the effect on the linear stability of a two-fluid, cylindrical Couette flow of jumps in fluid properties of varying magnitude, of variations in interfacial position, and of varying gap width is investigated.

2. The primary flow

Consider two infinitely long, concentric cylinders of radii $R_1 < R_2$ with two immiscible, viscous fluids of differing but constant densities, ρ_1, ρ_2, and kinematic viscosities, ν_1, ν_2, filling the annulus between them. Fluid 1 is to be found in $R_1 \leqslant r \leqslant R_s$ and fluid 2 in $R_s \leqslant r \leqslant R_2$, where R_s is the radius of the equilibrium fluid–fluid interface and r is the radius in the usual r, θ, z cylindrical co-ordinate system. The inner and outer cylinders are rotating independently with angular velocities Ω_1 and Ω_2, respectively. The equations describing the flow in each fluid region, ignoring surface tension, are given by

$$\rho D\mathbf{v}/Dt + \nabla p = \operatorname{div}(\rho\nu \operatorname{def}\mathbf{v}), \quad (\operatorname{def}\mathbf{v} \equiv (\operatorname{grad}\mathbf{v}) + (\operatorname{grad}\mathbf{v})^*) \tag{1}$$

$$\nabla . \mathbf{v} = 0, \tag{2}$$

$$D\rho/Dt = 0, \tag{3}$$

$$DR_s/Dt = v_r(R_s), \tag{4}$$

where t is time, $D/Dt = \partial/\partial t + \mathbf{v}.\nabla$ is the substantial derivative, p is pressure, $\mathbf{v}$ the vector velocity, and v_r the radial component of velocity. (An asterisk denotes the transpose of a tensor.) Definition of the problem is completed by the non-slip boundary conditions at $r = R_1, R_s, R_2$ and the continuity-of-shear condition at $r = R_s$.

We now seek a solution of this system of equations and boundary conditions which is independent of time and has only an azimuthal velocity component varying solely with the radius. Proceeding as in the single-fluid case, we find that such a solution exists and can be written in the form

$$V(r) = \begin{cases} V_1(r) = A_1 r + B_1/r & (R_1 \leqslant r \leqslant R_s), \\ V_2(r) = A_2 r + B_2/r & (R_s \leqslant r \leqslant R_2), \end{cases} \tag{5}$$

where A_1, A_2, B_1, and B_2, are given, by virtue of the boundary conditions, as

$$\left.\begin{aligned} A_1 &= \frac{\Omega_1\left\{\gamma n - 1 + \left(\frac{x_s+\Delta}{1+\Delta}\right)^2 - \gamma n\omega\left(\frac{x_s+\Delta}{\Delta}\right)^2\right\}}{\gamma n - 1 + \left(\frac{x_s+\Delta}{1+\Delta}\right)^2 - \gamma n\left(\frac{x_s+\Delta}{\Delta}\right)^2}, \\ A_2 &= \frac{\Omega_1\left\{\omega(\gamma n - 1) + \left(\frac{x_s+\Delta}{1+\Delta}\right)^2 - \gamma n\omega\left(\frac{x_s+\Delta}{\Delta}\right)^2\right\}}{\gamma n - 1 + \left(\frac{x_s+\Delta}{1+\Delta}\right)^2 - \gamma n\left(\frac{x_s+\Delta}{\Delta}\right)^2}; \end{aligned}\right\} \tag{6a}$$

$$\left.\begin{aligned} B_1 &= \frac{\gamma n(\omega - 1)\, l^2\Omega_1(x_s+\Delta)^2}{\gamma n - 1 + \left(\frac{x_s+\Delta}{1+\Delta}\right)^2 - \gamma n\left(\frac{x_s+\Delta}{\Delta}\right)^2}, \\ B_2 &= \frac{(\omega - 1)\, l^2\Omega_1(x_s+\Delta)^2}{\gamma n - 1 + \left(\frac{x_s+\Delta}{1+\Delta}\right)^2 - \gamma n\left(\frac{x_s+\Delta}{\Delta}\right)^2}, \end{aligned}\right\} \tag{6b}$$

where

$$\gamma = \rho_2/\rho_1, \quad n = \nu_2/\nu_1, \quad \omega = \Omega_2/\Omega_1, \quad l = R_2 - R_1, \quad \Delta = R_1/l, \quad x_s = (R_s - R_1)/l.$$

The corresponding pressure distribution is given within each region by

$$dp/dr = \rho V^2(r)/r \tag{7}$$

but it disappears from the stability problem and need not be determined explicitly.†

† In the presence of a constant axial pressure gradient, $\partial p/\partial z$, and any constant axial body force, $F_z(= -\rho g$, for example), there is superimposed on the azimuthal motion an axial velocity distribution of the form

$$v_z = C + D\ln r + (1/4\mu)\,(\partial p/\partial z - F_z)\, r^2,$$

where C and D are constants, different within each fluid region. It is this velocity that has been assumed small enough so that it contributes a stabilizing effect only, and thus may be neglected.

3. The perturbation equations

If we perturb about stationary values, linearize the scalar equivalents of (1)–(4) about the stationary values, and then assume normal mode decompositions for the perturbations of the form†

$$\mathbf{v} \equiv (v_r, v_\theta, v_z) = (u(r)\cos kz, V(r)+v(r)\cos kz, w(r)\sin kz)\exp(st+im\theta), \quad \text{(i)}$$

$$\left\{\begin{matrix}\rho\\ p\\ R_s\end{matrix}\right\} = \left\{\begin{matrix}\rho\\ p\\ R_s\end{matrix}\right\} + \left\{\begin{matrix}\delta\rho\\ \delta\pi\\ r_s\end{matrix}\right\}\cos kz\exp(st+im\theta), \quad \text{(ii)}$$

we obtain the following set of linear perturbation equations, after subtracting the corresponding equations for the stationary quantities,

$$D^*u = -\{im(v/r)+kw\}, \quad (8)$$

$$\left(s+\frac{imV(r)}{r}\right)\delta\rho = 0, \quad (9)$$

$$\left(s+\frac{imV(R_s)}{R_s}\right)r_s = u(R_s), \quad (10)$$

$$\nu\left\{DD^*-\left(\frac{m^2}{r^2}+\frac{imV(r)}{r\nu}+k^2+\frac{s}{\nu}\right)\right\}u(r)-\frac{D(\delta\pi)}{\rho} = -\left\{\frac{V^2(r)}{\rho r}\right\}\delta\rho-\left\{\frac{2}{r}\left(V(r)-\frac{im\nu}{r}\right)\right\}v(r), \quad (11)$$

$$\nu\left\{DD^*-\left(\frac{m^2}{r^2}+\frac{imV(r)}{r\nu}+k^2+\frac{s}{\nu}\right)\right\}v(r) = \left\{D^*V-\frac{2im\nu}{r^2}\right\}u(r)+\left(\frac{im}{\rho r}\right)\delta\pi(r), \quad (12)$$

$$\nu\left\{D^*D-\left(\frac{m^2}{r^2}+\frac{imV(r)}{r\nu}+k^2+\frac{s}{\nu}\right)\right\}w(r) = -\left(\frac{k}{\rho}\right)\delta\pi(r), \quad (13)$$

where $$D \equiv d/dr \quad \text{and} \quad D^* \equiv (d/dr)+(1/r),$$

k is real, m is a real integer, and s is a complex number whose real part determines stability and imaginary part overstability.

By assumption $\delta\rho = 0$ *within* each fluid region, so (9) is identically satisfied and (11) reduces to

$$\nu\left\{DD^*-\left(\frac{m^2}{r^2}+\frac{imV(r)}{r\nu}+k^2+\frac{s}{\nu}\right)\right\}u(r) = \frac{D(\delta\pi)}{\rho}-2\left\{V(r)-\frac{im\nu}{r}\right\}\frac{v(r)}{r}. \quad (11a)$$

The bracketed term in (10) vanishes only if $m = s \equiv 0$. For the two-fluid case this implies $u(R_s) = 0$, so that $r_s = 0$, since no corrugation can exist without a velocity component normal to the interface. If $m \neq 0$ or $s \neq 0$ (10) can be solved for r_s,

$$r_s = \frac{u(R_s)R_s}{sR_s+imV(R_s)}. \quad (10a)$$

† In some cases we have used the same symbol for the whole variable and its stationary part. This should cause no confusion since the whole variables henceforth do not appear.

Using (10a), r_s can be eliminated wherever it appears so that the remaining equations are (8), (11a), (12), and (13), a set of four equations with four unknowns.

Let us now define functions Y_j in region 1 ($R_1 \leqslant r \leqslant R_s$) and Z_j in region 2 ($R_s \leqslant r \leqslant R_2$) as follows:

$$Y_1 = \frac{u_1}{R_1\Omega_1}, \quad Y_2 = \frac{v_1}{R_1\Omega_1 l}, \quad Y_3 = \frac{aw_1}{R_1\Omega_1}, \quad Y_4 = -\left(\frac{imv_1}{R_1\Omega_1 l} + \frac{axw_1}{R_1\Omega_1} + \frac{lx\delta\pi_1}{\rho_1\nu_1 R_1\Omega_1}\right),$$

$$Y_5 = \frac{x^2}{R_1\Omega_1} D\left(\frac{v_1}{x}\right), \quad Y_6 = \frac{ax}{R_1\Omega_1} Dw_1; \quad Z_1 = \frac{u_2}{R_1\Omega_1}, \quad Z_2 = \frac{v_2}{R_1\Omega_1 l}, \quad Z_3 = \frac{aw_2}{R_1\Omega_1},$$

$$Z_4 = -\left(\frac{imv_2}{R_1\Omega_1 l} + \frac{axw_2}{R_1\Omega_1} + \frac{lx\delta\pi_2}{\rho_2\nu_2 R_1\Omega_1}\right), \quad Z_5 = \frac{x^2}{R_1\Omega_1} D\left(\frac{v_2}{x}\right), \quad Z_6 = \frac{ax}{R_1\Omega_1} Dw_2,$$

where $a \equiv kl$, $i \equiv \sqrt{-1}$, $D \equiv d/dx$, $x = r/l$. Then (8), (11a), (12) and (13) can be decomposed as shown below:

$$DZ_1 = -(Z_1 + imZ_2)/x - Z_3, \tag{14}$$

$$DZ_2 = (Z_2 + Z_5)/x, \tag{15}$$

$$DZ_3 = Z_6/x, \tag{16}$$

$$DZ_4 = xM_2(x)\, Z_1 + \left\{\frac{2im}{x} + \frac{\sqrt{T'}}{n}\left(\alpha x + \frac{\beta_2}{x}\right)\right\} Z_2 + Z_4/x, \tag{17}$$

$$DZ_5 = -\frac{x}{n}\left\{\alpha\sqrt{T'} + \frac{2imn}{x^2}\right\} Z_1 + x\left\{\left(\frac{m}{x}\right)^2 + M_2(x)\right\} Z_2 - im(Z_3 + Z_4/x) - Z_5/x, \tag{18}$$

$$DZ_6 = ima^2 Z_2 + x\{a^2 + M_2(x)\}\, Z_3 + a^2 Z_4; \tag{19}$$

all of which are valid for $1 + \Delta \geqslant x > x_s + \Delta$, and

$$DY_1 = -(Y_1 + imY_2)/x - Y_3, \tag{20}$$

$$DY_2 = (Y_2 + Y_5)/x, \tag{21}$$

$$DY_3 = Y_6/x, \tag{22}$$

$$DY_4 = xM_1(x)\, Y_1 + \left\{\frac{2im}{x} + \sqrt{T'}\left(x + \frac{\beta_1}{x}\right)\right\} Y_2 + Y_4/x, \tag{23}$$

$$DY_5 = -x\left\{\sqrt{T'} + \frac{2im}{x^2}\right\} Y_1 + x\left\{\left(\frac{m}{x}\right)^2 + M_1(x)\right\} Y_2 - im(Y_3 + Y_4/x) - Y_5/x, \tag{24}$$

$$DY_6 = ima^2 Y_2 + x\{a^2 + M_1(x)\}\, Y_3 + a^2 Y_4; \tag{25}$$

which are valid for $x_s + \Delta > x \geqslant \Delta$. In the above the following definitions have been used:

$$\alpha = A_2/A_1, \ \beta_1 = B_1/A_1 l^2, \ \beta_2 = B_2/A_1 l^2, \ T = \text{Taylor number} = -4A_1\Omega_1 l^4/\nu_1^2,$$
$$T' = -A_1 T/\Omega_1, \quad M_1(x) = (m/x)^2 + a^2 + i(\bar{c} - \tfrac{1}{2}m\sqrt{T'}\{1 + (\beta_1/x^2)\}), \tag{26}$$
$$M_2(x) = (m/x)^2 + a^2 + i/n(\bar{c} - \tfrac{1}{2}m\sqrt{T'}\{\alpha + (\beta_2/x^2)\}), \quad \bar{c} = \text{Im}\,(s)\, l^2/\nu_1.$$

Also, since we are only interested in neutral stability limits, we have set Re $(s) = 0$. (Im ( ) stands for 'imaginary part of' and Re ( ) for 'real part of').

Equations (14)–(19) and (20)–(25) constitute the perturbation equations in a form convenient for numerical integration.

4. The boundary conditions

The boundary conditions at the cylindrical surfaces are, in the new notation,

$$Z_1(1+\Delta) = Z_2(1+\Delta) = Z_3(1+\Delta) = 0, \tag{27}$$

$$Y_1(\Delta) = Y_2(\Delta) = Y_3(\Delta) = 0. \tag{28}$$

The 'no-slip' condition at the fluid–fluid interface is more complicated because the position of the interface has also been perturbed. Using Taylor series expansions about the unperturbed interface location and the assumption of small perturbations, one can show (Schneyer 1968) that continuity of the vector velocity at the interface yields the conditions:

$$Y_1 = Z_1, \quad Y_2 = Z_2 + \tfrac{1}{2}i\left[\frac{\sqrt{T'}}{\bar{c}+m\bar{V}/(x_s+\Delta)}\right]\times\left[\alpha - 1 + \frac{\beta_1-\beta_2}{(x_s+\Delta)^2}\right]Z_1, \quad Y_3 = Z_3, \tag{29}$$

where all functions are evaluated at $x = x_s+\Delta$, and

$$\bar{V}(x_s+\Delta) = -\tfrac{1}{2}\sqrt{T'}\{(x_s+\Delta)+\beta_1/(x_s+\Delta)\}.$$

Equations (27)–(29) are sufficient boundary conditions for the sixth-order system, (14)–(19) and (20)–(25). The fact that they are in the form of conditions for a two-point eigenvalue problem makes them inconvenient to use numerically. We therefore use them, and the differential equations, to generate a full set of six initial conditions for each region in the manner of Harris & Reid (1964), Krueger *et al.* (1966), and many others. In this solution scheme, advantage is taken of the linearity of the system to determine three arbitrary, orthogonal solution vectors, a linear combination of which determines the linear manifold of all solution vectors with the three given initial conditions. Thus, only the three additional boundary conditions left unspecified at the fluid–fluid interface $(x_s+\Delta)$, which are to become initial conditions, need be determined. The details of the derivation are given in Schneyer (1968); the results are

$$\left.\begin{aligned} Y_4 = \gamma n Z_4 - \left\{2(\gamma n-1) - \frac{i(\gamma-1)\,\bar{V}^2}{\bar{c}+m\bar{V}/(x_s+\Delta)}\right\}Z_1 \\ + im(Y_2-\gamma n Z_2) - (\gamma n-1)\,(x_s+\Delta)\,Z_3, \\ Y_5 = \gamma n Z_5 - im(\gamma n-1)\,Z_1, \; Y_6 = \gamma n Z_6 - a^2(\gamma n-1)\,(x_s+\Delta)\,Z_1, \end{aligned}\right\} \tag{30}$$

where all functions are evaluated at $x = x_s+\Delta$. We note that if $m = \bar{c} \equiv 0$, two changes in conditions (29) and (30) occur; the modified conditions are

$$Y_2(x_s+\Delta) = Z_2(x_s+\Delta), \tag{29a}$$

$$Y_4(x_s+\Delta) = \gamma n Z_4(x_s+\Delta) - (\gamma n-1)\{2Z_1(x_s+\Delta) + (x_s+\Delta)\,Z_3(x_s+\Delta)\}. \tag{30a}$$

5. Method of solution

A perusal of (14)–(25) shows that there is a pole at $x = 0$. Increased numerical accuracy can be achieved, therefore, by performing the integration from $x = 1+\Delta$ to $x = \Delta$ rather than vice versa. Thus, (14)–(19) are integrated from $x = 1+\Delta$ to $x = x_s+\Delta$, starting with (27) and one of Z_4, Z_5, Z_6 set equal to one and the others zero, as initial conditions. Using (29) and (30), the Z_j's are related to the Y_j's across the fluid–fluid interface at $x_s+\Delta$; these relations then form the initial conditions for (20)–(25) to be integrated to $x = \Delta$. This procedure is repeated twice more with different initial condition vectors at $x = 1+\Delta$. Because of the homogeneity of the required conditions at $x = \Delta$, a necessary condition for the existence of a solution is

$$\begin{vmatrix} Y_1^{(1)}(\Delta) & Y_1^{(2)}(\Delta) & Y_1^{(3)}(\Delta) \\ Y_2^{(1)}(\Delta) & Y_2^{(2)}(\Delta) & Y_2^{(3)}(\Delta) \\ Y_3^{(1)}(\Delta) & Y_3^{(2)}(\Delta) & Y_3^{(3)}(\Delta) \end{vmatrix} \equiv 0, \tag{31}$$

where the superscripts denote the three cases having differing initial condition vectors. Equation (31) can be written, symbolically, as the complex equation

$$F(m, a, \bar{c}, T) = 0. \tag{31a}$$

For a given m and a, we shall denote by $(T_e, \bar{c}_e)$ any combination of T and $\bar{c}$ which satisfies (31) (or (31a)); this combination constitutes the 'complex eigenvalue' of the system.† Since the minimum T_e over all possible values of m and a is the quantity physically observed, we shall denote the minimum T_e over all possible values of a (and its associated $\bar{c}_e$) by $(T_a, \bar{c}_a)$, while the minimum T_a over all possible values of m (and its associated $\bar{c}_a$) will be denoted by $(T_c, \bar{c}_c)$.

The actual computational scheme is given in detail in Schneyer (1968) and represents a slight modification of the numerical scheme described in Krueger, Gross & Di Prima (1966). The calculations were carried out in single-precision, floating-point arithmetic on a CDC 6400 using a fifth-order Runge–Kutta integration scheme with variable step size and a Gaussian elimination determinant-evaluation scheme. A comparison of results due to Krueger, Gross & Di Prima (1966) (denoted by a subscript K), Roberts (1965) (denoted by a subscript R), and the authors (denoted by a subscript S) is shown in table 1. Only the last two, starred, cases shown in the table differ by more than the quoted accuracy of Krueger, Gross & Di Prima (± 2 in the fourth significant figure), and $T_S = 3509{\cdot}71$ is closer to $T_R = 3509{\cdot}52$ than is $T_K = 3509{\cdot}9$, although Roberts claims significance for all six digits. As a result, it is believed that one can have confidence in at least three significant figures in T, $\bar{c}$, and a, and possibly a fourth significant figure in T and $\bar{c}$ if $T < 50{,}000$.

† The mathematical eigenvalue, for real m and a, is $c = c_r + i\bar{c}$ and T is only a parameter, but setting $c_r \equiv 0$, in order to calculate the neutral stability limits, has made $(T, \bar{c})$ the new 'eigenvalue' for the problem. Furthermore, while the equations and boundary conditions clearly indicate that $T' = (-A_1/\Omega_1)T$ would be a more 'proper' parameter, T has been used for historical and comparison purposes.

ω	m_c	a	T_K	T_S	T_R	$\bar{c}_K$	$\bar{c}_S$
0	0	3·128	3,509·9	3,509·7	3,509·52	0	0
−0·8	3	3·561	13,730	13,728·2	—	−15·106	−15·1057
−1·0	4	3·680	20,072	20,067·9	—	−23·358	−23·3576
−1·25	5	3·774	30,632	30,622·3	—	−33·102	−33·1032
−1·5	6	4·002	45,307	45,289·8	—	−43·616	−43·6182
−1·75*	6	3·986	65,411	65,370·2	—	−51·537	−51·5340
−2·0*	7	4·483	91,298	91,234·8	—	−64·147	−64·1567

TABLE 1. Comparison of results for the case $\gamma = 1$, $n = 1$, $\eta = 0{\cdot}95$

6. Results and conclusions

The results of our calculations are neutral stability curves, and consequently only results for stably stratified flows ($\gamma \geqslant 1$) are presented. This limitation eliminates the possibility of a Rayleigh–Taylor instability. There are five physical parameters (γ, n, ω, x_s, $\eta \equiv R_1/R_2$) of interest. Because of this large number, specific values of these parameters have been chosen to constitute a 'base' case ($\gamma = 2$, $n = \frac{3}{4}$, $\omega = 0$, $x_s = \frac{1}{2}$, $\eta = 0{\cdot}95$) from which nearly all parameter variations originate. Thus, the variation of a parameter has usually been analyzed by varying only that parameter in the 'base' case. Because several single-fluid investigations (Chandrasekhar 1961; Pao 1966; and Krueger, Gross & Di Prima 1966; for instance) have considered the variations in T_c and associated parameters with changing ω (at least for $-1 \leqslant \omega \leqslant 1$), only the case $\omega = 0$ is treated here.

It has been found that for a given azimuthal wave-number, m, the 'eigenvalues' trace out a *curve* in $T_e - \bar{c}_e - a$ space. For most cases the curve has a shallow trough-like shape which is only slightly skewed out of a $\bar{c}_e$ = constant plane. In the course of investigating the effect of changing density ratio, γ, the existence of modes (multiple 'eigenvalues') has been uncovered by the calculation of two different sets of $(T_e, \bar{c}_e)$ for identical wave-numbers. Except for a few 'anomalous' cases, which will be discussed in detail later, the modes are easily characterized by their positions along the $\bar{c}_e$ axis; that is, the mode whose curve lies near the more negative $\bar{c}_e$ is characterized as 'mode I' while that lying near the more positive $\bar{c}_e$ is denoted as 'mode II'. Projections of a $T_e - \bar{c}_e - a$ modal curve ($T_e - a$ curves) for a representative case is shown in figure 1. The modal relationship of the curves in figure 1 is somewhat atypical insofar as the Taylor number of the controlling mode (the mode with a smaller T_a) for nearly all cases has been found to occur at a lower axial wave-number a as well. This results in the usual modal curves having minima which exhibit a wider separation than shown in the figure.

Figure 2 shows the two sets of modal 'eigenvalues' found for the cases $1 \leqslant \gamma \leqslant 2$, $n = 1$, $\omega = 0$, $x_s = \frac{1}{2}$, $\eta = 0{\cdot}95$, $m = 1$. From these results one may conclude that: (*a*) Only two modes exist. The manner in which the two sets of modal 'eigenvalues' smoothly approach the single-fluid 'eigenvalue', which is known to be unique (see Chandrasekhar 1961, for instance), combined with the complete absence of any evidence of a third 'eigenvalue', even for γ only slightly

above unity, very strongly suggests such a conclusion. (*b*) The instability phenomenon being observed is a Taylor cylindrical Couette instability for both modes. This conclusion is also based on the single-fluid result—a Taylor phenomenon—being smoothly approached. In fact, the similarity evident among the curves in $T_e - \bar{c}_e - a$ space for all but the 'anomalous' cases and the manner in which, for most cases, they have smoothly evolved from single-fluid results indicates that nearly all the results obtained are due to Taylor phenomena. (*c*) The stability of the system, as measured by T_a or T_c, increases with increasing γ, at least with regard to the Taylor instability. This result is probably due to the increased inertia effecting an angular momentum instability.

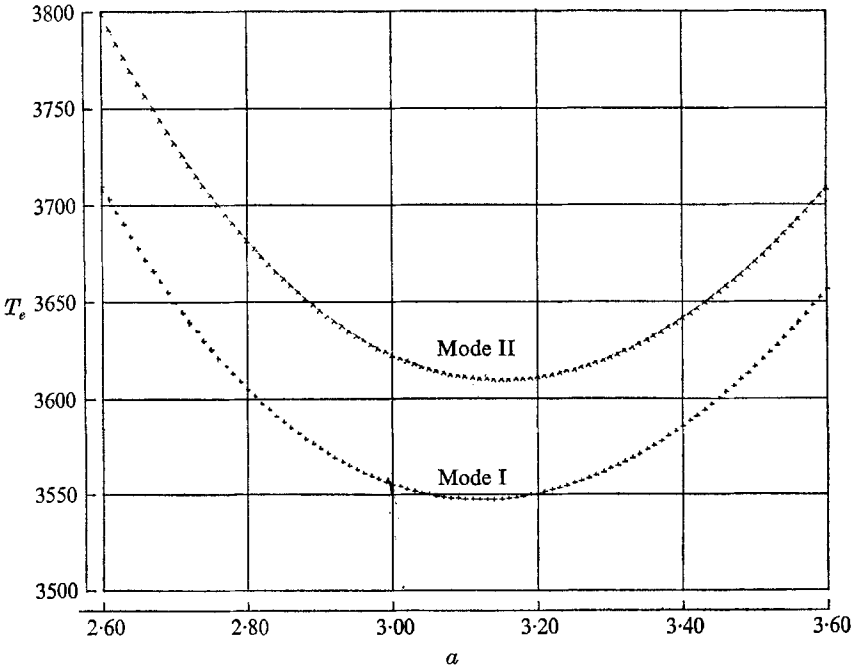

FIGURE 1. Taylor number *vs.* axial wave-number for both modes of $\gamma = 1{\cdot}01$, $n = 1$, $\omega = 0$, $\eta = 0{\cdot}95$, $x_s = \frac{1}{2}$, $m = 1$.

Figure 3 shows the results for the cases $1 \leqslant \gamma \leqslant 1{\cdot}5$, $n = \frac{3}{4}$, $\omega = 0$, $x_s = \frac{1}{2}$, $\eta = 0{\cdot}95$, $m = 1$. The two modes are seen to exist for all $\gamma \geqslant 1$ and even show a differing behaviour for the smaller γ. As a result, it is obvious that the modes represent a two-fluid phenomenon rather than one due to jumps in kinematic or dynamic viscosity or density alone.

The physical origin of the two modes cannot be conclusively proved, but it is believed they are manifestations of the classical Taylor instability phenomenon in each of the two fluids separately, modified from single-fluid results by the interfacial-boundary interaction of the fluids. If this interpretation is correct, figure 2 seems to indicate that mode I corresponds to fluid 1 and mode II to fluid 2, since it is the inertia of fluid 2 which is increased by raising γ.

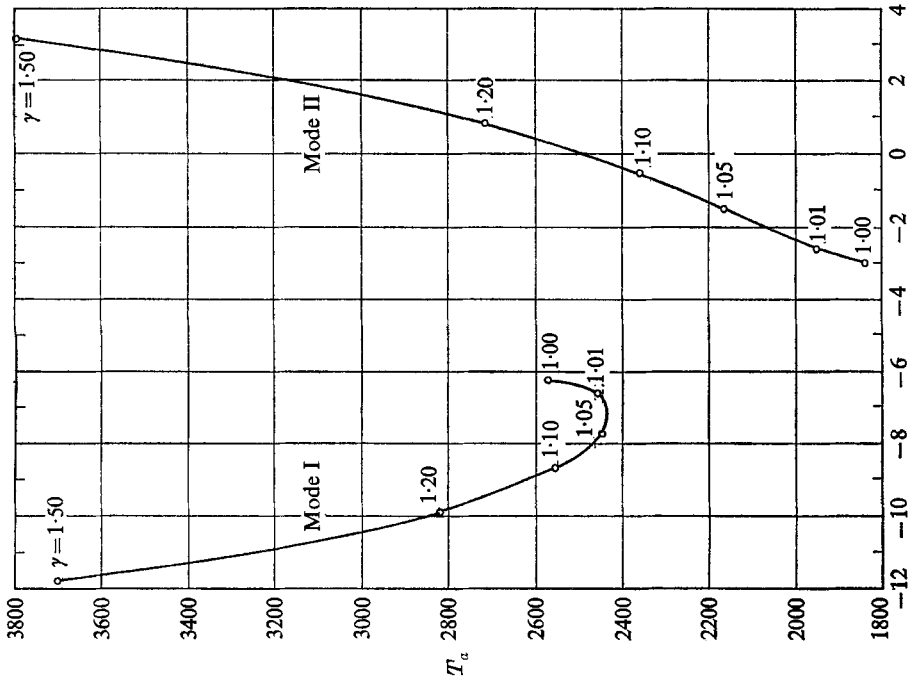

FIGURE 3. Minimum 'eigenvalues' as a function of density ratio for both modes of $n = \frac{3}{4}$, $\omega = 0$, $x_s = \frac{1}{2}$, $\eta = 0{\cdot}95$, $m = 1$.

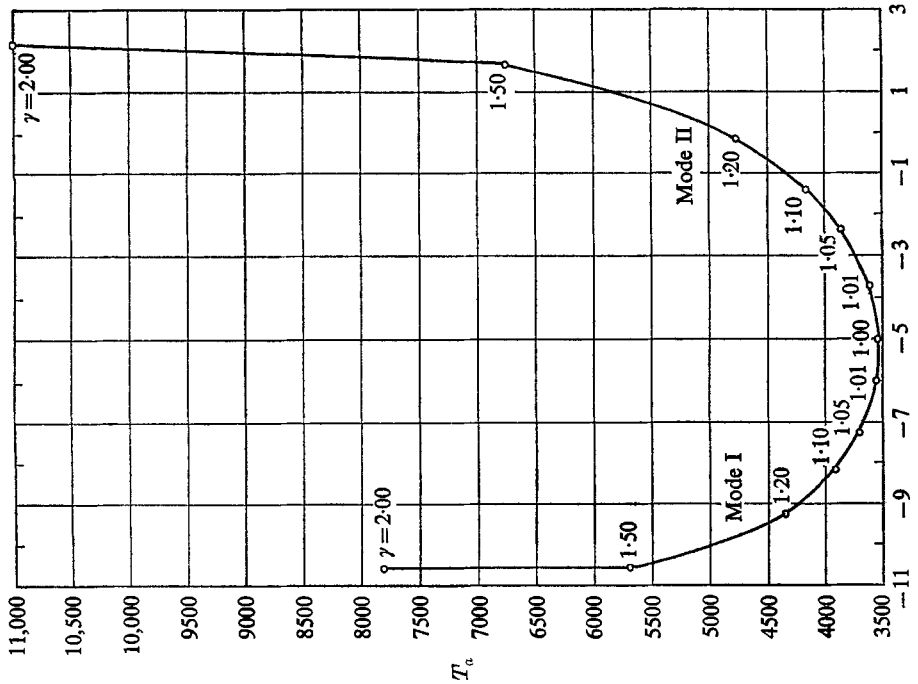

FIGURE 2. Minimum 'eigenvalues' as a function of density ratio for both modes of $n = 1$, $\omega = 0$, $x_s = \frac{1}{2}$, $\eta = 0{\cdot}95$, $m = 1$.

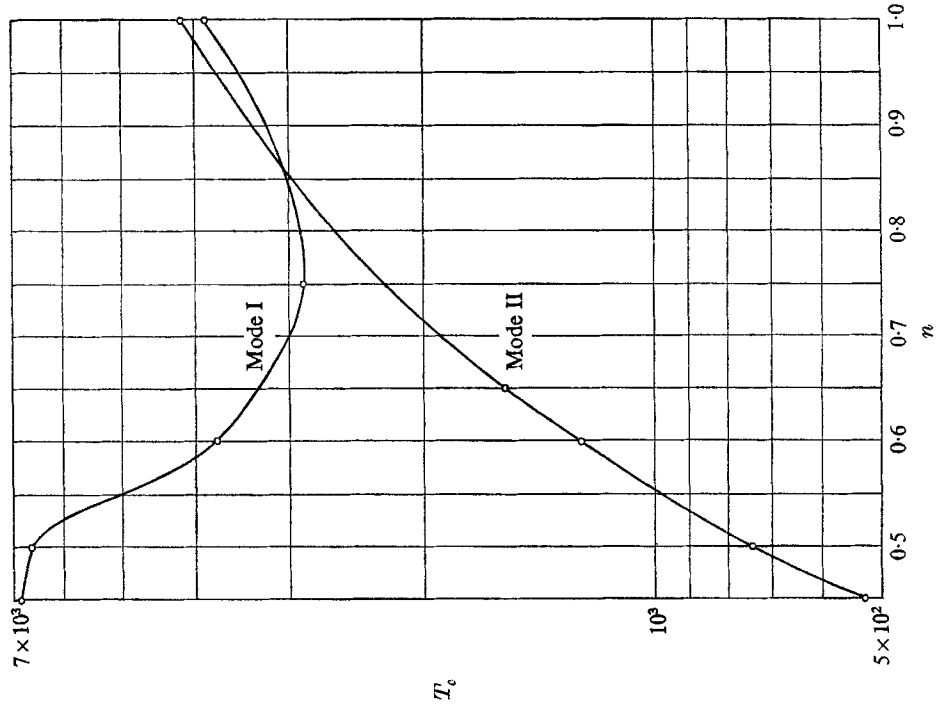

FIGURE 5. Critical Taylor number *vs.* kinematic viscosity ratio for both modes of $\gamma = 1{\cdot}1$, $\omega = 0$, $x_s = \frac{1}{2}$, $\eta = 0{\cdot}95$.

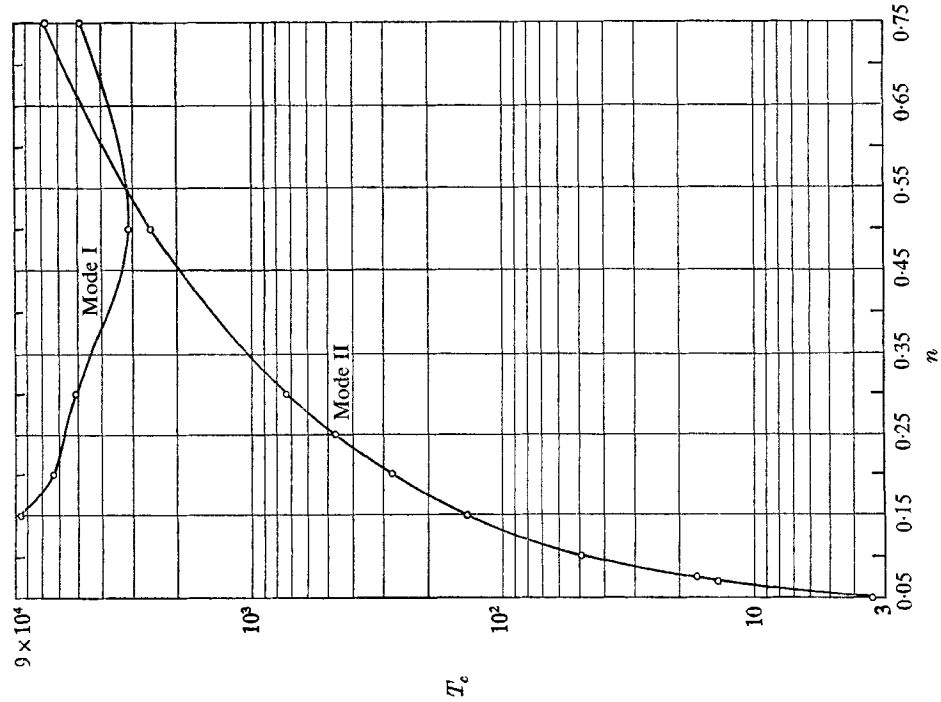

FIGURE 4. Critical Taylor number *vs.* kinematic viscosity ratio for both modes of $\gamma = 2$, $\omega = 0$, $x_s = \frac{1}{2}$, $\eta = 0{\cdot}95$.

Finally, the shift in controlling mode from I to II as γ increases in figure 3 occurs around $\gamma n = 1$ ($\gamma = \frac{4}{3}$). This would seem to indicate that the dynamic viscosity ratio is the dominant influence in determining the controlling mode. A possible explanation for this result may be found in Rayleigh's inviscid criterion, which, while not correct for viscous fluids, should indicate the proper trend. Thus, while Γ^2 is always decreasing with increasing radius for the $\omega = 0$ case, $\gamma n < 1$ causes a sudden, rapid decrease in Γ^2 on the fluid 2 side of the fluid–fluid interface, while $\gamma n > 1$ puts the more severe condition in fluid 1. If the relationship between fluids and modes discussed above is correct, mode I should be the controlling mode for large γn and mode II should control for small γn, with the crossover occurring around $\gamma n = 1$. This is the condition observed in figures 3, 4 and 5, with only the exact value of γn at which the crossover occurs varying among the three cases.

η	m	$T_{a\mathrm{I}}$	$\bar{c}_{\mathrm{I}}$	a_{I}	$T_{a\mathrm{II}}$	$\bar{c}_{\mathrm{II}}$	a_{II}
0·95	3	4,926·8	−20·60	2·92	6,765·5	−3·83	3·41
0·95	4	4,865·8	−24·60	2·86	7,449·6	−8·59	3·51
0·95	5	4,854·7	−28·71	2·80	8,268·7	−13·70	3·60
0·95	6	4,890·6	−32·97	2·73	9,185·3	−19·14	3·69
0·75	0	7,079·4	−8·34	3·15	7,079·4	+8·34	3·15
0·75	1	6,208·5	−17·86	2·95	9,704·9	−2·00	2·95
0·75	2	6,334·5	−28·80	2·90	15,129	−15·36	3·73
0·50	0	11,538	−6·80	3·19	11,538	+6·80	3·19
0·50	1	9,674·6	−23·64	2·95	44,097	−12·36	3·83
0·50	2	22,691	−67·77	3·33	49,582	−34·94	4·25
0·30	0	22,912	−3·08	3·24	22,912	+3·08	3·24
0·30	1	27,064	−36·94	3·21	132,823	−19·21	4·17
0·25	0	23,757	0	3·34	23,757	0	3·34
0·25	1	50,158	−47·96	3·18	—	—	—
0·24	1	59,882	−51·69	3·13	—	—	—
0·23	1	73,956	−56·54	3·05	—	—	—
0·22	1	96,930	−63·59	2·92	—	—	—
0·215	1	117,000	−69·27	2·83	—	—	—
0·2125	1	134,292	−74·00	2·76	—	—	—
0·2110	1	157,750	−80·20	2·68	—	—	—
0·20	0	33,483	0	3·39	33,483	0	3·39
0·15	0	53,110	0	3·45	53,110	0	3·45
0·10	0	105,192	0	3·52	105,192	0	3·52
0·05	0	363,617	0	3·62	363,617	0	3·62

TABLE 2. Variation in minimum Taylor number and associated parameters for both modes with azimuthal wave-number and radius ratio for $\gamma = 2$, $n = \frac{3}{4}$, $\omega = 0$, $x_s = \frac{1}{2}$

The variation in T_c with η is shown in figure 6 and table 2. The results exhibit two striking characteristics. The first and foremost is the monotonic increase in T_c with increasing gap width (decreasing η). An explanation for this trend again can be found in the effect of increasing gap width on $D(\Gamma^2)$ through its effect on the slope of the steady velocity profile. Since $T^{\frac{1}{2}} \sim \Omega_1$, an increase in Taylor number steepens the steady velocity profile. Thus, a rising T can balance an increase in gap width and result in the restoration or maintenance of neutral stability.

The other striking characteristic is the progressive trend with increasing gap width towards a stationary 'donut' vortex ($m = 0, \bar{c} = 0$) as the critical instability. Although such a result has been found in all single-fluid investigations when $\omega = 0$, the results of the present investigation indicate that it is a rare occurrence in the two-fluid case. The probable explanation lies in the decreasing influence exerted by one fluid on the instability mechanism of the other, due to the increased distance from the fluid–fluid interface to the 'site' of the perturbation. This explanation assumes, of course, the hypothesized fluid-mode relationship, but is supported by the fact that *both* modes exhibit the same behaviour.

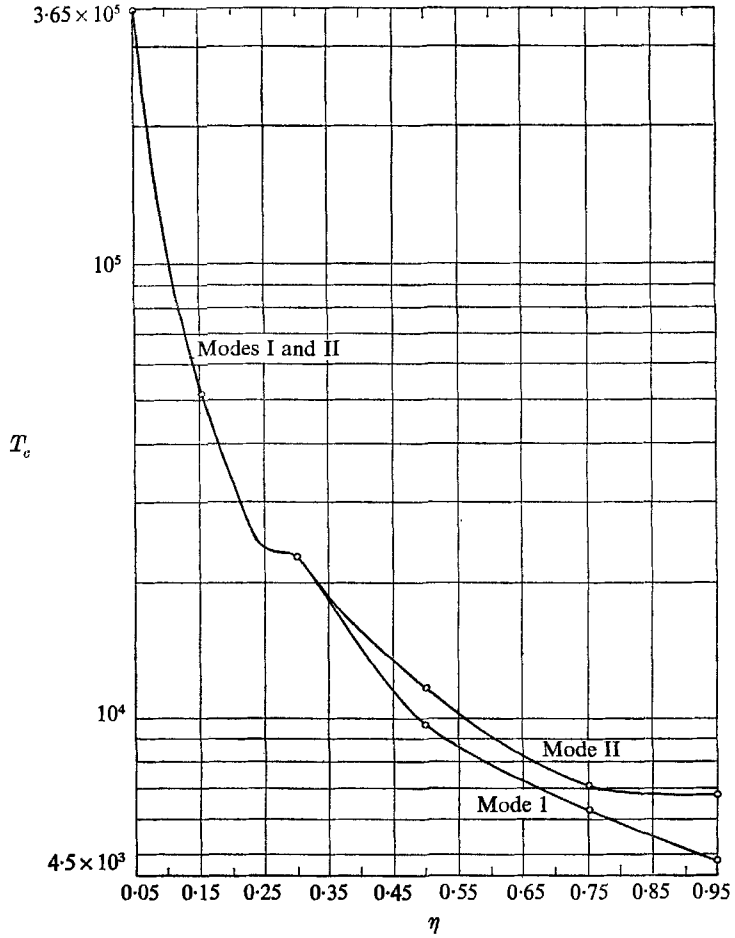

FIGURE 6. Critical Taylor number *vs.* radius ratio for both modes of $\gamma = 2$, $n = \frac{3}{4}$, $\omega = 0$, $x_s = \frac{1}{2}$.

From all of the above discussion it seems clear that only Taylor phenomena have manifested themselves here. The shape of the $T_c - a$ curves and the continuous variation in 'eigenvalues' from a single-fluid, Taylor 'eigenvalue' definitely indicate this. Any other 'eigenvalues' which may exist and are

attributable to some other mechanism must lie in a different, unsearched region of 'eigenvalue' space and must await further analytic investigation.

It should be noted here that when $m = 0$ one always finds that the modes are related by $T_{a_{\mathrm{I}}} = T_{a_{\mathrm{II}}}$, $a_{\mathrm{I}} = a_{\mathrm{II}}$, and $\bar{c}_{\mathrm{I}} = -\bar{c}_{\mathrm{II}}$.† More generally, taking the complex conjugate of (26)–(42), one finds that the equations are invariant if $T \to T$, $a^2 \to a^2$, $m \to -m$, $\bar{c} \to -\bar{c}$. In fact, for the general ($c_r \neq 0$) case, the equations remain invariant if $T \to T$, $a^2 \to a^2$, $m \to -m$, $c \to c^*$, so that if $c = c_r + i\bar{c}$ is an eigenvalue for T, $\pm a$, and m, then $c^* = c_r - i\bar{c}$ is an eigenvalue for T, $\pm a$, $-m$. Thus, the observed phenomenon is simply a special case of the above eigenvalue relation.

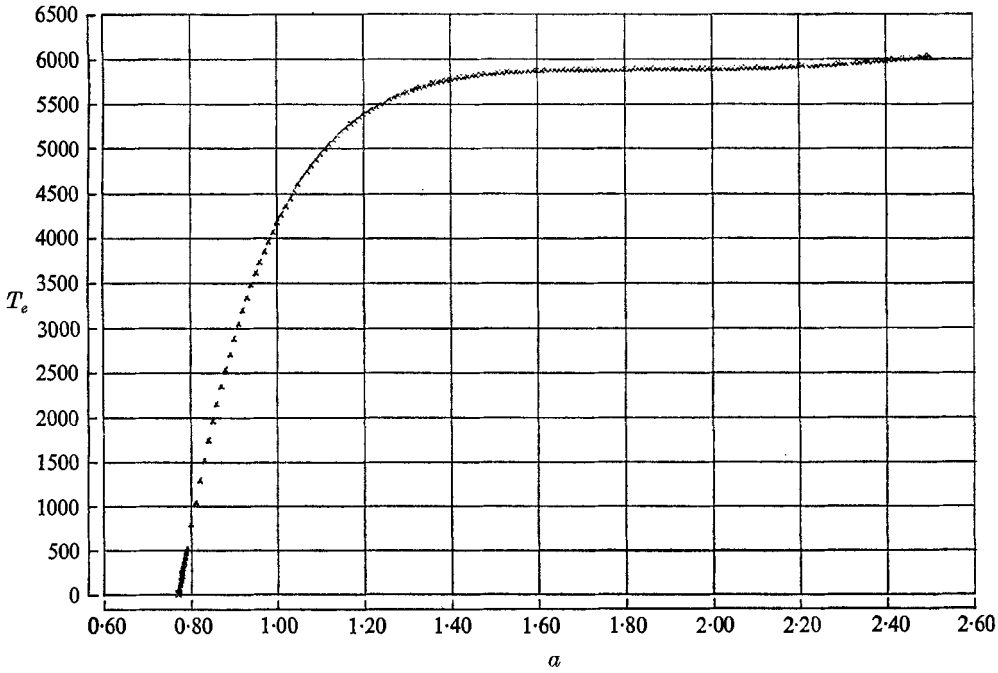

FIGURE 7. Taylor number *vs.* axial wave-number for 'anomalous' case of mode I, $\gamma = 2$, $n = 1$, $\omega = 0$, $\eta = 0{\cdot}95$, $x_s = \frac{1}{2}$, $m = 4$.

Figures 4 and 5 illustrate the variation in critical Taylor number with kinematic viscosity ratio, n, for density ratios of 2 and 1·1, respectively. Between them, they also illustrate the influence of the dynamic viscosity ratio, γn. It can be seen that the two curves are qualitatively very similar. As a result only the $\gamma = 2$ case has been thoroughly investigated. The investigation has revealed at least two 'anomalous' cases which, incidentally, are not shown in figure 4. The first such case has been discovered for $\gamma = 2, n = 1, m = 4$ (mode I), and has its $T_e - a$ curve shown in figure 7, while the second has been found for $\gamma = 2$, $n = 0{\cdot}045$, $m = 1$ (mode II). While not apparent in figure 7, the 'anomalous' $T_e - \bar{c}_e - a$ curve is very

† This result for $m = 0$, which follows from taking the complex conjugate of the governing equations and boundary conditions, was pointed out to the authors by Professor S. H. Davis in a private communication and led the authors to the formulation of the relationship for a general m which follows in the text.

three-dimensional in that the $\bar{c}_e$ spread is many times larger than that of a 'regular' curve for the same spread in a. We shall now discuss separately these two different sets of results, the 'regular' and the 'anomalous'.

Nearly all the explanations for the phenomena observed in varying viscosity for the 'regular' points have been given above. Thus, the fact that mode I is controlling at large γn while mode II controls at small γn has already been explained. The monotonic decrease in T_c with decreasing n (and γn) exhibited by mode II is probably also due to the accelerated decrease in Γ^2 which lies at the heart of that argument. On the other hand, the minimum exhibited by mode I at $\gamma n \approx 1$ can only be partially (i.e. for $\gamma n < 1$) explained by such an argument. The rise for $\gamma n > 1$ is probably due to the rise in the dissipative capability of the system which occurs as the viscosity increases.

The most obvious conclusion to be drawn from the 'regular' results is that stability is enhanced by increasing the kinematic viscosity ratio; that is, the Taylor cylindrical Couette phenomenon is stabilized by increasing n. This conclusion is based on the same phenomenological arguments used above to link the results to a Taylor phenomenon. In fact, any other phenomena which might have manifested themselves would probably not have exhibited the same $T_e - a$ characteristics and would have been classified 'anomalous'. We now turn to these phenomena.

The completely different character exhibited by the $T_e - \bar{c}_e - a$ curves of the 'anomalous' cases has led to the belief that they represent different phenomena, whose 'eigenvalues' were found because they happened to lie close enough to Taylor 'eigenvalues'. The most likely phenomena are the Kelvin–Helmholtz (K–H) and Yih instabilities, since they are possible mechanisms in the present model.

The K–H, or inviscid-shear, instability is known to be possible in parallel shear flows if and only if the steady velocity profile exhibits a 'shear-like character' (a continuous velocity profile of a homogeneous fluid exhibits a 'shear-like character' if its curvature undergoes a sign change). Since for the cases considered, $\alpha > 0$, $\beta_1 < 0$, and $\beta_2 < 0$, we find that $D\overline{V}_j < 0$ and $D^2\overline{V}_j > 0$. This represents a decelerating (with radius) flow whose deceleration rate is declining. The only possibility of generating a shear-type profile, therefore, lies in making $D\overline{V}_2$ more negative than $D\overline{V}_1$ at the fluid–fluid interface, which is exactly the situation for $\gamma n < 1$. It would appear, therefore, that one could not use the K–H instability to explain all the 'anomalous' results since half of them occur for $\gamma n > 1$. Stuart (1967), however, has suggested that the significance of the 'shear-like character' lies in the maximum in the associated vorticity profile which coincidentally occurs in parallel shear flows. For rotational flows this coincidence no longer exists. For the cases considered here, the vorticity is a constant within a fluid with the maximum occurring in the inner fluid for $\gamma n > 1$ and the outer fluid for $\gamma n < 1$. If one accepts the hypothesized relationship between the modes and the fluids, then all the 'anomalous' cases do in fact occur in the fluid with the larger vorticity. Thus, from this viewpoint, all of the 'anomalous' cases could be K–H instabilities.

The Yih, or viscosity-stratification, instability (Yih 1967), unfortunately, is not well understood. It seems to be similar to the K–H instability in that both

yield growing waves at the fluid–fluid interface, but the Yih instability is tied in an essential manner to the viscosity jump. Whether this tie is to be found in the type of steady velocity profile the jump imposes, in the dissipative or diffusive rate jumps that accompany a viscosity jump, in the distortion of a K–H stable profile to a K–H unstable profile by viscous action on the perturbed velocity

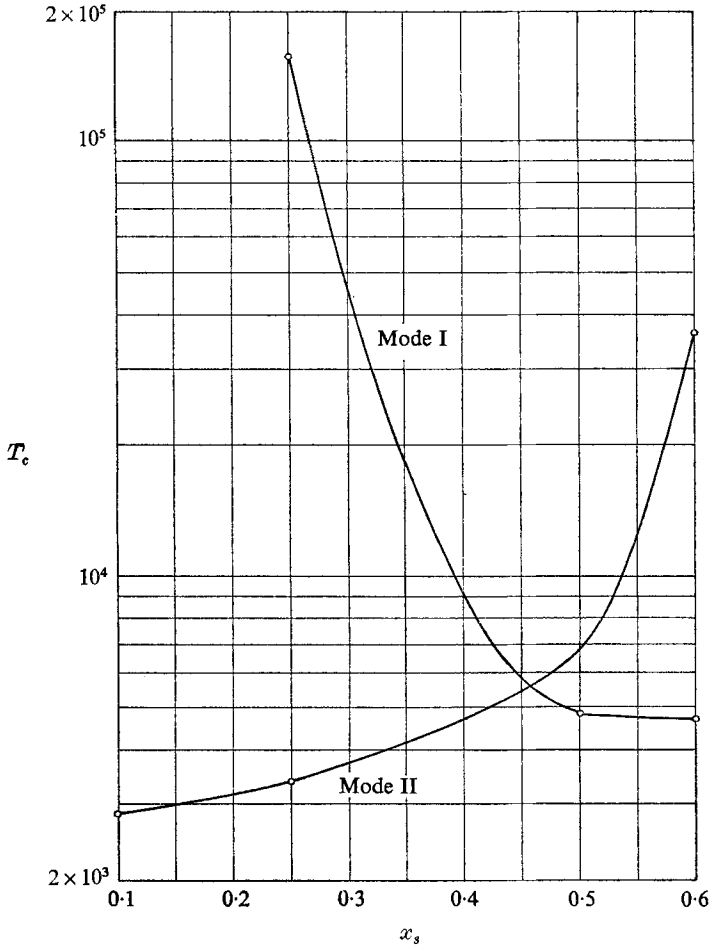

FIGURE 8. Critical Taylor number *vs.* interfacial position for both modes of $\gamma = 2$, $n = \frac{1}{4}$, $\omega = 0$, $\eta = 0{\cdot}95$.

profile, or in some other mechanism is not yet known. Furthermore, the dependence on wave-number is unclear since Yih (1967), in the only known investigation of this instability, chose to solve the problem by an analytic, small wave-number expansion technique with evaluation limited to the first two terms. On the other hand, the instability is known to occur for both K–H stable and K–H unstable steady velocity profiles. Thus, while detailed characteristics of the Yih instability are unknown, the fact that it is apparently not inhibited by the $\gamma n > 1$ condition makes it a possible source for all of the 'anomalous' cases.

Although only four 'anomalous' cases have been found among more than 100 cases evaluated, it seems likely that many 'anomalous' results remain

'buried' in remote (from the Taylor 'eigenvalue' region) areas of the 'eigenvalue' plane. Thus an analytic investigation of this problem might reveal many 'eigenvalues' whose existence has only been suggested here. All the cases for which $\gamma n < 1$, for instance, are potentially K–H unstable. The fact that the Taylor numbers associated with the cylindrical Couette instability are over 100 times larger than those of the 'anomalous' cases, for which, in general, unconditional instability is indicated by $T \to 0$ for sufficiently small a, emphasizes the importance of these hidden 'eigenvalues'. Thus, a further investigation of this problem seems warranted.†

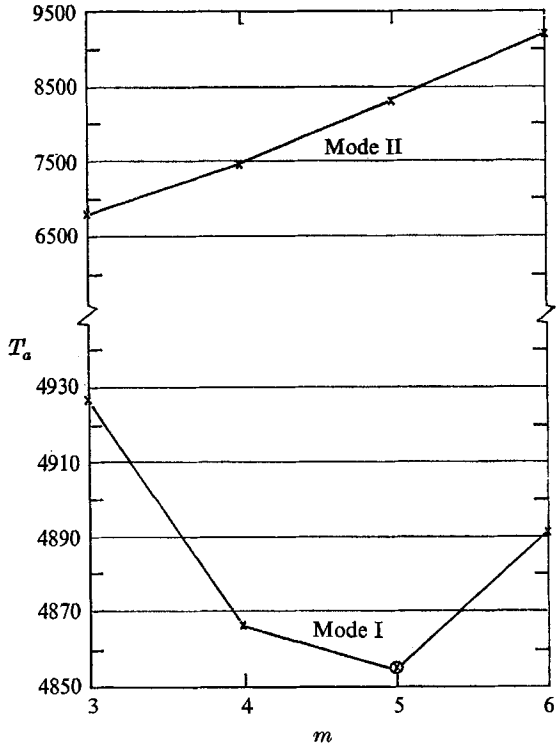

FIGURE 9. Minimum Taylor number *vs.* azimuthal wave-number for both modes of $\gamma = 2$, $n = \frac{3}{4}$, $\omega = 0$, $x_s = \frac{1}{2}$, $\eta = 0{\cdot}95$.

Figure 8 shows the variation in T_c with interfacial position. It indicates that one can equilibrate the modes by shifting the interfacial position. In general, decreasing x_s stabilizes mode I and destabilizes mode II and vice versa. Unfortunately, no adequate explanation for this behaviour has yet been found.

An 'anomalous' case has been uncovered for $\gamma = 2$, $n = \frac{3}{4}$, $\omega = 0$, $x_s = 0{\cdot}675$, $\eta = 0{\cdot}95$, $m = 1$ (mode I). This case is unique in that it exhibits both the general 'anomalous' behaviour of figure 7 while having a well defined critical Taylor

† Professor J. T. Stuart, in a private communication, has suggested that it might prove rewarding to consider the inviscid stability problem with the correct velocity profile. This should yield the K–H instabilities, at least. Determination of some of the eigenfunctions for both 'regular' and 'anomalous' cases might also prove quite revealing.

number of 24·018. The balance of forces which has resulted in a stable configuration for $T < 24$ is unknown.

In figures 9 and 10 are shown typical $T_a - m$ curves illustrating the well-defined minima (with $\otimes$ denoting T_c) for the controlling mode as well as the unification of the modes at $m = 0$.

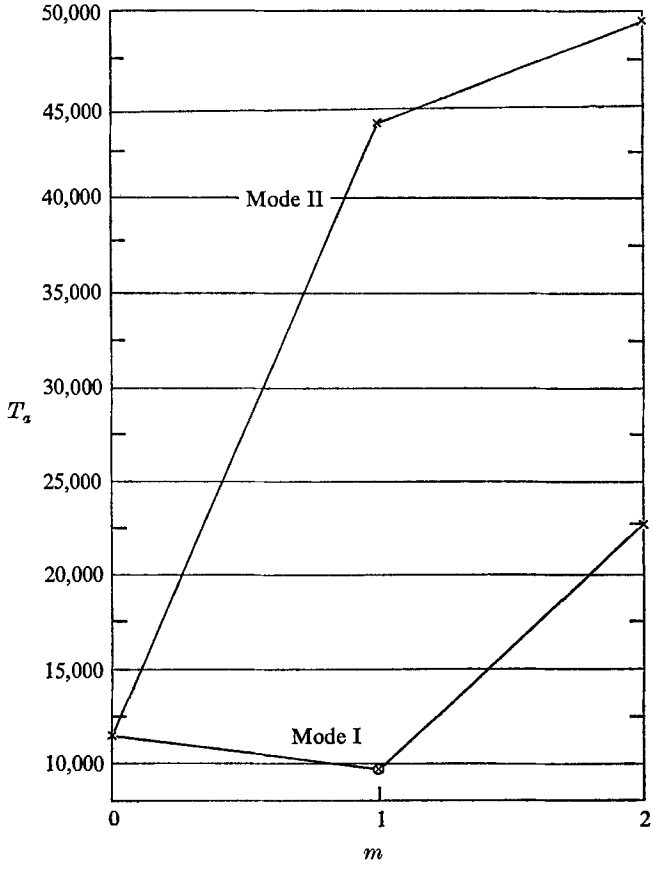

FIGURE 10. Minimum Taylor number *vs.* azimuthal wave-number for both modes of $\gamma = 2$, $n = \frac{3}{4}$, $\omega = 0$, $x_s = \frac{1}{2}$, $\eta = \frac{1}{2}$.

From the results discussed, it seems likely that the cylindrical Couette instability is not decisive in determining whether the proposed scheme could be used in a gas-core reactor. Determination of the origin of the 'anomalous' cases and their susceptibility to stabilization by an axial magnetic field therefore become the questions of major interest.

Many more results were obtained than could be presented in the figures and tables included in this article. A complete set of tables has been deposited with the Editor of the *Journal* and is available upon request.

One of the authors (G.P.S.) was partly supported, at differing times, by the Douglas Aircraft Company, Inc., under their Full-Time-Off Scholarship Program,

and by the Mechanics Branch, Office of Naval Research, under Contract Nonr-222(44). The University of California Computer Center at Berkeley supplied the necessary CDC 6400 computer time. We are indebted to Professors F. S. Sherman, D. R. Willis, F. Wolf, and S. H. Davis for their valuable suggestions and criticisms.

REFERENCES

CHANDRASEKHAR, S. 1961 *Hydrodynamic and Hydromagnetic Stability*. Oxford: Clarendon.

COLES, D. 1965 Transition in circular Couette flow. *J. Fluid Mech.* **21**, 385–426.

DAVEY, A., DI PRIMA, R. C. & STUART, J. T. 1968 On the instability of Taylor vortices. *J. Fluid Mech.* **31**, 17–52.

DI PRIMA, R. C. 1960 The stability of a viscous fluid between rotating cylinders with an axial flow. *J. Fluid Mech.* **9**, 621–31.

DONNELLY, R. J. & SCHWARZ, K. W. 1965 Experiments on the stability of viscous flow between rotating cylinders. VI. *Proc. Roy. Soc.* A **283**, 531–49.

GROSS, A. G. 1965 Numerical investigation of the stability of Couette flow. Ph.D. Thesis, Rensselaer Polytechnic Institute, Troy, N.Y.

HARRIS, D. L. & REID, W. H. 1964 On the stability of viscous flow between rotating cylinders. Part 2. Numerical analysis. *J. Fluid Mech.* **20**, 95–102.

HUGHES, T. H. & REID, W. H. 1968 The stability of spiral flow between rotating cylinders. *Phil. Trans. Roy. Soc.* A **263**, 57–91.

JOHNSON, K. 1966 A plasma-core nuclear rocket utilizing a magnetohydrodynamically-driven vortex. *A.I.A.A. J.* **4**, 635–43.

KRUEGER, E. R., GROSS, A. G. & DI PRIMA, R. C. 1966 On the relative importance of Taylor-vortex and non-axisymmetric modes in flow between rotating cylinders. *J. Fluid Mech.* **24**, 521–38.

PAO, H. S. 1966 Further results on stability of a swirling fluid with variable density in the presence of a circular magnetic field. *Phys. Fluids*, **9**, 1254–5.

RAYLEIGH, LORD 1920 On the dynamics of revolving fluids. *Scientific Papers*, **6**, 447–53.

RESHOTKO, E. & MONNIN, C. F. 1965 Stability of two-fluid wheel flows. *NASA TN* D-2696.

ROBERTS, P. H. 1965 The solution of the characteristic value problems. Appendix to Experiments on the stability of viscous flow between rotating cylinders. VI. *Proc. Roy. Soc.* A **283**, 550–6.

SCHNEYER, G. P. 1968 Linear hydrodynamic and hydromagnetic stability of the dissipative, two-fluid cylindrical Couette problem. Ph.D. Thesis, published as *University of California, Berkeley Aero. Sci. Rep.* AS-68-12.

SNYDER, H. A. & LAMBERT, R. B. 1966 Harmonic generation in Taylor vortices between rotating cylinders. *J. Fluid Mech.* **26**, 545–62.

SPARROW, E. M., MUNRO, W. D. & JONSSON, V. K. 1964 Instability of the flow between rotating cylinders: The wide gap problem. *J. Fluid Mech.* **20**, 35–46.

STUART, J. T. 1967 Hydrodynamic stability of fluid flows. *Inaugural Lectures, London: The Imperial College of Science and Technology*, 111–116.

TAYLOR, G. I. 1923 Stability of a viscous liquid contained between two rotating cylinders. *Phil. Trans. Roy. Soc.* A **223**, 289–343.

WALOWIT, J., TSAO, S. & DI PRIMA, R. C. 1964 Stability of flow between arbitrarily spaced concentric cylindrical surfaces including the effect of a radial temperature gradient. *J. Appl. Mech.* **31**, 585–93.

YIH, C. S. 1961 Dual role of viscosity in the instability of revolving fluids of variable density. *Phys. Fluids*, **4**, 806–11.

YIH, C. S. 1967 Instability due to viscosity stratification. *J. Fluid Mech.* **27**, 337–352.